



RESEARCH ARTICLE

High-power, widely wavelength-tunable, single-frequency pulsed fiber master oscillator power amplifier at 2.8 μm

Zongxiao Fan^{1,†}, Wenshu Liu^{1,†}, Zhehao Wu¹, Shengyi Wang², Huimin Yue¹, Chen Wei^{1,3}, and Yong Liu¹

¹State Key Laboratory of Electronic Thin Films and Integrated Devices, School of Optoelectronic Science and Engineering, University of Electronic Science and Technology of China, Chengdu, China

²School of Electronics and Information, Northwestern Polytechnical University, Xi'an, China

³Tianfu Jiangxi Laboratory, Chengdu, China

(Received 28 October 2024; revised 20 December 2024; accepted 23 January 2025)

Abstract

We present a high-power mid-infrared single-frequency pulsed fiber laser (SFPFL) with a tunable wavelength range from 2712.3 to 2793.2 nm. The single-frequency operation is achieved through a compound cavity design that incorporates a germanium etalon and a diffraction grating, resulting in an exceptionally narrow seed linewidth of approximately 780 kHz. Employing a master oscillator power amplifier configuration, we attain a maximum average output power of 2.6 W at 2789.4 nm, with a pulse repetition rate of 173 kHz, a pulse energy of 15 μJ and a narrow linewidth of approximately 850 kHz. This achievement underscores the potential of the mid-infrared SFPFL system for applications requiring high coherence and high power, such as high-resolution molecular spectroscopy, precision chemical identification and nonlinear frequency conversion.

Keywords: high-power lasers; mid-infrared lasers; pulsed lasers; single frequency

1. Introduction

The single-frequency pulsed fiber laser (SFPFL), distinguished by its exceptional attributes of narrow linewidth, high coherence, high pulse energy and versatility^[1–4], has garnered significant attention across a wide range of applications such as high-resolution spectroscopy, coherent LIDAR, chemical identification and optical frequency combs generation^[5–9]. Of particular interest is the SFPFL source operating in the mid-infrared spectral region, where the essential vibrational–rotational spectral bands of numerous light molecules are found^[10]. This specific capability, coupled with the laser's potential for high power output and broadband tunability, bestows upon it unparalleled advantages in diverse fields. Notably, in biomedical research where non-invasive diagnostics are paramount, together with nonlinear optics for efficient frequency conversion processes and environmental monitoring through sensitive trace-gas

detection techniques, the high-power SFPFL emerges as a pivotal tool, driving advancements and opening new avenues for exploration and innovation^[11,12].

Generally, single-frequency operation in fiber lasers can be achieved through several wavelength selection approaches, such as enhancing the free spectral range (FSR) of the resonant cavity via advanced configurations such as compound cavities^[13], ring cavities^[14] and ultra-short cavities^[15]. In addition, the integration of narrowband filtering elements such as ultra-narrow fiber Bragg gratings (FBGs)^[16], saturable absorbers (SAs)^[17] and other sophisticated wavelength-selective optics plays a crucial role. To date, several mid-infrared single-frequency fiber lasers have been demonstrated. By employing FBGs in ultra-short cavities (~ 0.1 m), where the FSR is significantly enhanced to approximately 1 GHz, single-frequency operations were achieved at 2.8 μm ^[18] and 2.9 μm ^[19]. In longer cavities (~ 1 m), meticulous utilization of high-precision optical components (e.g., germanium (Ge) etalon and diffraction grating) within compound cavity designs introduces stringent wavelength selectivity. This approach not only secures single-frequency laser output but also bestows wavelength tunability spanning from 2.7 to 2.8 μm ^[20], 2.9 to

Correspondence to: C. Wei, State Key Laboratory of Electronic Thin Films and Integrated Devices, School of Optoelectronic Science and Engineering, University of Electronic Science and Technology of China, Chengdu 611731, China. E-mail: cwei@uestc.edu.cn

[†]These authors contributed equally to this work.

3.2 μm ^[21] and an extended range of 3.3–3.7 μm ^[2], thereby broadening the applicability and versatility of these lasers in various scientific and technological contexts.

However, the average output powers of these mid-infrared single-frequency fiber lasers are limited to the milliwatt level, a constraint primarily stemming from inherent design and material limitations. In ultra-short cavities, the restricted length of active fiber and the low dopant concentrations severely cap both laser gain and pump absorption efficiency, thereby posing formidable obstacles to achieving high output powers and broad wavelength tunability. Conversely, in longer cavities, while an extended active fiber length theoretically enhances pump absorption and laser gain, the reliance on high-precision optical components introduces substantial insertion loss into the cavity. This not only diminishes the overall efficiency but also suppresses wavelength selectivity under conditions of high-power operation^[2], effectively hindering the achievable power scaling of single-frequency laser emissions. Furthermore, the absence of effective modulation mechanisms has limited these mid-infrared single-frequency fiber lasers within continuous-wave (CW) operations, thereby compromising their potential in numerous high-impact applications that necessitate powerful, pulsed laser sources. These include defense technologies, nonlinear frequency conversion processes and long-range remote sensing capabilities, where high-power single-frequency laser sources functioning in pulsed operation are instrumental. The generation of pulsed lasers fundamentally revolves around two principal methodologies: active and passive modulation. Within the specific context of mid-infrared fiber lasers, particularly those operating around the 3 μm spectral region, passive modulation techniques, especially those employing SAs, have emerged as a prevalent and widely adopted technique^[22,23]. Nonetheless, despite the potential for achieving high-pulse-energy SFPFLs through the implementation of SAs, this approach is not without its own set of challenges. The insertion losses introduced by the incorporation of SAs, alongside concerns regarding their thermal damage thresholds, impose significant limitations on the achievable power scaling.

Confronted with the constraints imposed by various factors previously discussed, the enhancement of output power of mid-infrared SFPFLs necessitates an effective power scaling approach. The master oscillator power amplifier (MOPA) configuration, which has been ubiquitously leveraged across different spectral ranges – including SFPFL systems operating at 1 μm ^[24], 1.5 μm ^[25] and 2 μm ^[26], as well as non-SFPFL platforms at 2.3 μm ^[27] and 2.8 μm ^[28,29] – stands out as a prime candidate for addressing this issue. This is attributed to its proven ability to substantially enhance both the average power and the energy per pulse of laser emissions, thereby offering a viable pathway to overcome the inherent limitations and achieve enhanced performance in mid-infrared SFPFL systems. Within the

MOPA configurations, high-power SFPFLs have been achieved with average powers of hundreds of watts at 1 μm ^[30] and kilowatt-level peak powers at 1.5 μm ^[31] and 2 μm ^[32]. Nevertheless, there has been an absence of reported instances of high-power mid-infrared SFPFLs to date.

In this work, we demonstrated a high-power mid-infrared wavelength-tunable SFPFL based on a single-stage MOPA architecture operating around 2.8 μm . This system achieved a wavelength tuning range of 80.9 nm, spanning from 2712.3 to 2793.2 nm, with a maximum average output power reaching 2.6 W at a repetition rate of 173 kHz, corresponding to a pulse energy of 15 μJ . The single-frequency operation was meticulously ensured through the integration of a Ge etalon and a diffraction grating within our compound cavity design. The verification of such operation was confirmed via beat-frequency spectroscopy and linewidth measurements using a strong coherent envelope technique with short delay, manifesting a narrow linewidth of less than 1 MHz.

2. Experimental setup

The experimental setup for the single-frequency *Q*-switched Er^{3+} -doped ZBLAN fiber seed laser and its amplifier is illustrated in Figure 1. The seed source is pumped by a 976 nm laser diode (LD) equipped with a fiber pigtail, featuring a core diameter of 105 μm and a numerical aperture (NA) of 0.22. The pump light is first collimated by an aspheric condenser lens (L1) with a focal length of 8 mm and a transmittance of 90% at 976 nm, and then focused by a ZnSe lens (L2) with a focal length of 12 mm and transmittances of 70% at 976 nm and 98% at 2.8 μm . The gain medium is a 0.9 m long, double-clad 7% (molar fraction) Er^{3+} -doped ZBLAN fiber with a core diameter of 15 μm , an NA of 0.12 and an inner cladding dimension of 240 μm \times 260 μm with an NA of 0.4. Both ends of the fiber are perpendicularly cleaved. The laser emitted from the opposite side of the fiber is collimated through L3, which shares the same specifications as L2. Subsequently, the laser beam is focused onto a Fe:ZnSe crystal and collimated via a pair of ZnSe lenses (L4 and L5), each with a focal length of 40 mm and a transmittance of 95% at 2.8 μm . A diffraction grating (Thorlabs, GR1325-45031) is employed to reflect the first-order diffracted beam for optical feedback. In conjunction with the wavelength selectivity of the grating and the compound cavity design, a Ge etalon with a thickness of 5 mm (Thorlabs, WG91050) is placed between L3 and L4 to further narrow the linewidth of the operating laser. A dichroic mirror (DM1), with a transmittance of 96% at 976 nm and a reflectivity of 95% at 2.8 μm , is placed at a 45° angle between L1 and L2 to direct the laser beam. After passing through a quarter-wave plate and a half-wave plate, the seed is reflected by a gold mirror (GM) placed at 45° into a polarization-dependent isolator (Faraday Photonics),

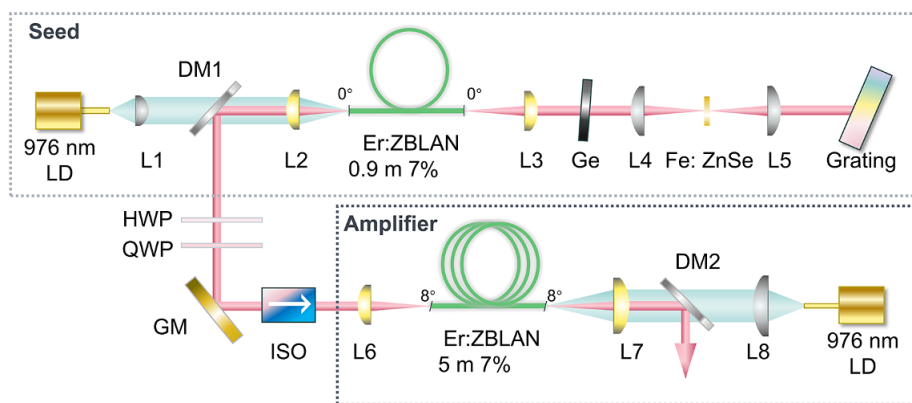


Figure 1. Schematic setup of the single-frequency Q -switched Er^{3+} -doped ZBLAN fiber MOPA laser system.

aimed at maximizing the transmission of the seed through the isolator while preventing oscillator dynamic disruption. The seed is then focused by L6, a ZnSe lens with a focal length of 12 mm and a transmittance of 98% at $2.8 \mu\text{m}$, into a 5 m long, double-clad 7% (molar fraction) Er^{3+} -doped ZBLAN fiber with a coupling efficiency of 70%. This gain fiber is cleaved at an angle of 8° at both ends and shares the characteristics of the one utilized in the seed system. A pair of ZnSe lens (L7), with transmittances of 70% at 976 nm and 95% at $2.8 \mu\text{m}$ and a focal length of 25 mm, and a CaF_2 lens (L8), with a transmittance of 90% at 976 nm and a focal length of 50 mm, is employed on the opposite side of the fiber to collimate and focus the amplified laser beam and the pump source from another 976 nm LD. To direct the output laser beam, DM2 is positioned at a 45° angle between L7 and L8, sharing the same transmittance and reflectivity properties as DM1.

The average output power was determined using a commercial power sensor (Thorlabs, S425C). The characteristics of the Q -switched pulse train and its corresponding radio frequency (RF) spectrum were assessed with a high-speed indium arsenide (InAs) detector (Judson, J12D) featuring a response time of 2 ns, connected to a digital oscilloscope (Siglent, SDS5034X) with a 350 MHz bandwidth, and an RF spectrum analyzer (AV4033A). The optical spectrum was recorded using an optical spectrum analyzer (OSA) (Yokogawa, AQ6377) offering a spectral resolution of 0.5 nm .

3. Results and discussion

3.1. Seed laser

Single-frequency operation was accomplished through the combined frequency selection of a Ge etalon, featuring a free spectral range (FSR) of approximately 8 GHz and a transmission bandwidth of approximately 1 GHz, a diffraction grating and the compound cavity

design. The compound cavity consists of the gain fiber itself ($\sim 0.9 \text{ m}$, FSR of $\sim 111 \text{ MHz}$) and a section from the pump end of the gain fiber to the grating ($\sim 1.1 \text{ m}$, FSR of $\sim 90 \text{ MHz}$), expanding the FSR of the compound cavity to 9.9 GHz. Through the synergistic frequency-selective action of these components and mechanisms, the resultant FSR of the entire laser system will be further broadened, thereby facilitating single-frequency operation. Stable Q -switching was realized using a Fe:ZnSe crystal as the SA, which has been utilized to enable robust and stable mid-infrared Q -switched operation under high-power conditions^[33].

The stable single-frequency Q -switched seed laser's characteristics were evaluated at a consistent launched pump power of 1.4 W, as shown in Figure 2. This corresponds to an average output power of 63 mW, with a repetition rate of 173 kHz and a pulse duration of $0.62 \mu\text{s}$ (Figure 2(a)). The optical spectrum is presented in Figure 2(b), showing a wavelength centered at 2789.6 nm. The full-width at half-maximum (FWHM) is approximately 0.5 nm, constrained by the resolution of the OSA (0.5 nm). An RF signal-to-noise ratio (SNR) of 45 dB, shown in the inset of Figure 2(b), indicates the high stability of the seed laser. Single-frequency operation was further validated using the beat-frequency method, as demonstrated in Figure 2(c). Within a 1.5 GHz range, no signal was detected except for the one at 0 MHz, confirming the single-frequency mode of the seed laser. To determine the linewidth of the seed laser, the second peak–valley difference (SPVD) of a self-homodyne coherent envelope was chosen as the metric to characterize the laser linewidth^[34,35]. As depicted in Figure 2(d), the SPVD value is found to be 17.8 dB. With a delay length of approximately 2.8 m, the corresponding linewidth can be calculated to be approximately 780 kHz, which yields a time–bandwidth product of approximately 0.48 for the SFPFL pulse, a value notably proximate to the theoretical limit of 0.44 for transform-limited Gaussian pulses. This narrow linewidth further validates the single-frequency operation.

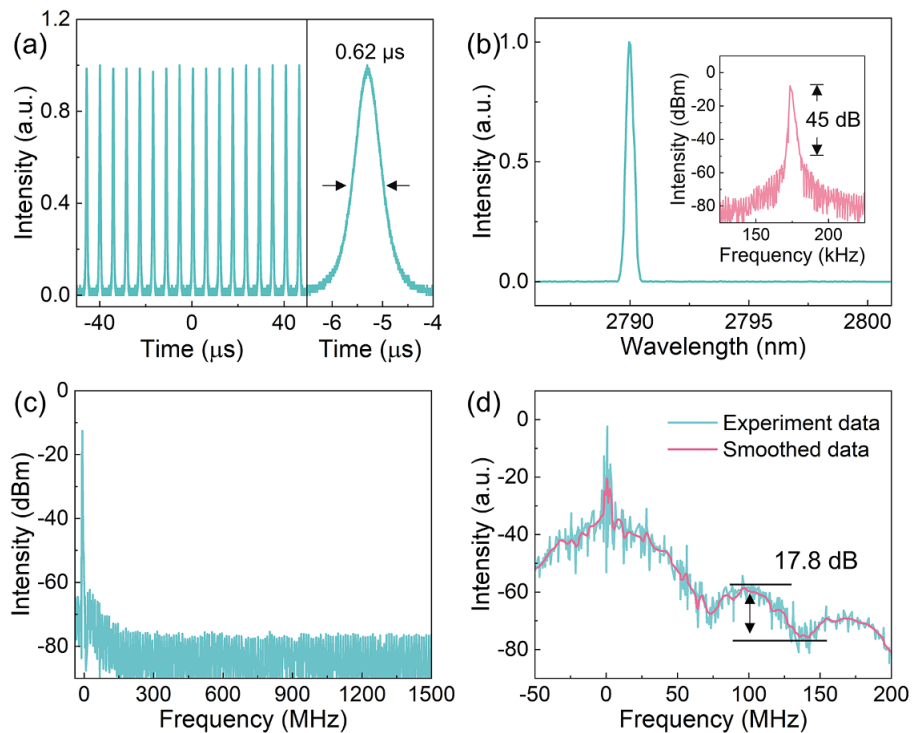


Figure 2. Characterization of the seed laser at a fixed launched pump power of 1.4 W: (a) Q -switched pulse train; (b) optical spectrum and RF spectrum (inset); (c) beat-frequency spectrum; (d) laser linewidth measured by employing a self-homodyne method with a short delay.

3.2. Amplifier

With the seed laser operating in a stable single-frequency Q -switching mode, approximately 30 mW of the signal was coupled into the fiber following its passage through the isolator and additional optical components. The output of the amplifier was characterized when operating at a launched pump power of 5.8 W. To investigate the tuning capability of this amplifier, we meticulously adjusted the angle of the diffraction grating, with the results depicted in Figure 3(a). Starting at the wavelength of 2712.3 nm, the average output power progressively increased from 0.93 W, reaching a peak of 1.26 W at 2789.4 nm, before declining to 1.17 W at 2793.2 nm. Throughout this tuning process, the laser system maintained stable single-frequency Q -switched operation. Notably, the variance in the average output power of the seed during wavelength tuning was less than 5 mW, suggesting that the efficiency of laser generation is optimal at the wavelength of 2789.4 nm. Further measurements and experiments were conducted at this wavelength.

The optical spectra of the seed (represented by the dashed blue curve) and the amplifier (solid pink curve) are depicted in Figure 3(b). Centered around 2789 nm, the optical spectra of the seed and amplifier present a fine degree of consistency. The inset of Figure 3(b) displays the beat-frequency spectrum, where no signal is detected except at 0 MHz, confirming the single-frequency operation of the amplifier. The linewidth was determined using the self-homodyne

method with a short delay (~ 2.8 m) employed in the seed configuration. As shown in Figure 3(c), the SPVD value is characterized to be 16.9 dB, which corresponds to an actual linewidth of approximately 850 kHz, 70 kHz broader than the linewidth of the seed. This slight broadening of the linewidth may be attributable to nonlinear effects (e.g., self-phase modulation^[36]) during the amplification process and the influence of amplified spontaneous emission^[37]. The pulse of the amplified laser is also documented in Figure 3(d). The repetition rate of 173 kHz matches that of the seed laser, while the pulse duration is 0.57 μ s. With the measured linewidth and pulse duration, the corresponding time–bandwidth product of the amplified laser is approximately 0.49, which approximates the limit of the time–bandwidth product inherent in a transform-limited Gaussian pulse. The long-term stability of the measured average output power was assessed over a 1-hour period at a pump power of 8.5 W, as depicted in Figure 3(e). The root-mean-square (RMS) deviation of less than 1% manifests the long-term stability of this single-frequency Q -switched MOPA system. Moreover, the amplified average output power and pulse energy were also measured in response to varying launched pump power to determine the maximum achievable output. As observed in Figure 3(f), both the average output power and pulse energy increase nearly linearly with respect to the launched pump power. The maximum average output power of 2.6 W and pulse energy of 15 μ J are achieved when the launched pump power reaches 10.5 W, corresponding

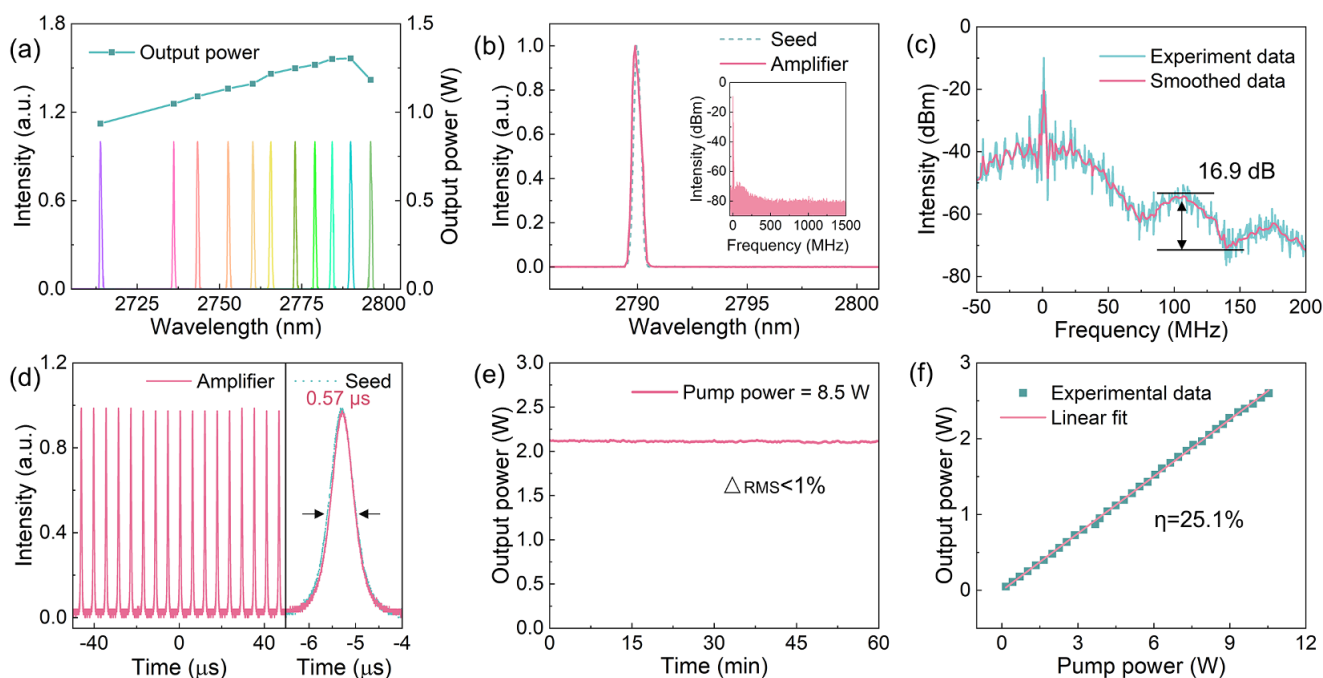


Figure 3. Characterization of the amplified laser output: (a) output power and optical spectrum as a function of wavelength; (b) optical spectrum and beat-frequency spectrum (inset); (c) laser linewidth measured by employing a self-homodyne method with a short delay; (d) Q -switched pulse train; (e) long-term stability of the output power; (f) output power as a function of the launched pump power.

to an amplification efficiency of 25.1%. However, a further enhancement in the launched pump power resulted in a sharp decline in output power, likely due to thermal damage on the fiber tip. In light of the absence of active cooling mechanisms in this MOPA system, further optimization measures, such as the incorporation of water cooling, could be implemented to further boost the output power.

4. Conclusion

In conclusion, we have successfully demonstrated a high-power, tunable SFPFL operating in the mid-infrared region. The MOPA architecture has been effectively employed to achieve a remarkable average output power of 2.6 W, with a stable single-frequency operation and a broad tuning range. The system's performance is further characterized by the narrow linewidth of approximately 780 kHz (seed) and approximately 850 kHz (amplifier), underpinning its suitability for high-precision applications. The scalability of the output power and the maintenance of single-frequency pulsed operation highlight the potential of this SFPFL for advanced photonic applications, including but not limited to spectroscopic analysis, remote sensing and nonlinear frequency conversion. Future improvements can be anticipated by optimizing the system for higher power outputs, potentially through the incorporation of active cooling mechanisms and multi-stage amplification in cavity design. This development signifies a significant advancement in the field

of mid-infrared SFPFLs and paves the way for new possibilities to achieve mid-infrared SFPFLs with high power.

Acknowledgements

This work was supported by the National Natural Science Foundation of China (Grant Nos. 62375041, 52203134 and 62075032) and the Fundamental Research Funds for the Central Universities (Grant No. ZYGX2019J051).

References

1. M. Leigh, W. Shi, J. Zong, J. Wang, S. Jiang, and N. Peyghambarian, *Opt. Lett.* **32**, 897 (2007).
2. L. Zhang, S. Fu, Q. Sheng, X. Luo, J. Zhang, W. Shi, and J. Yao, *Opt. Lett.* **48**, 6200 (2023).
3. Z. Zhou, Z. Wang, W. Huang, Y. Cui, H. Li, M. Wang, X. Xi, S. Gao, and Y. Wang, *Light Sci. Appl.* **11**, 15 (2022).
4. J. Geng, Q. Wang, J. Smith, T. Luo, F. Amzajerjian, and S. Jiang, *Opt. Lett.* **34**, 3713 (2009).
5. A. Hugi, G. Villares, S. Blaser, H. C. Liu, and J. Faist, *Nature* **492**, 229 (2012).
6. A. Schliesser, N. Picqué, and T. W. Hänsch, *Nat. Photonics* **6**, 440 (2012).
7. Y. Liu, J. Liu, and W. Chen, *Chin. Opt. Lett.* **9**, 090604 (2011).
8. O. Mhibik, S. Forget, D. Ott, G. Venus, I. Divliansky, L. Glebov, and S. Chénais, *Light Sci. Appl.* **5**, e16026 (2016).
9. C. Wei, L. Zhou, D. Wang, H. Chi, H. Huang, H. Zhang, and Y. Liu, *Photonics Res.* **8**, 972 (2020).
10. F. Keilmann, C. Gohle, and R. Holzwarth, *Opt. Lett.* **29**, 1542 (2004).

11. M. K. Shukla and R. Das, *IEEE J. Select. Topics Quantum Electronics* **24**, 5100206 (2018).
12. D. D. Arslanov, M. Spunei, J. Mandon, S. M. Cristescu, S. T. Persijn, and F. J. M. Harren, *Laser Photonics Rev.* **7**, 188 (2013).
13. H. Tan, F. Yan, T. Feng, T. Li, Q. Qin, D. Yang, H. Guo, X. Wang, G. Wu, Y. Cai, Y. Suo, Y. Bai, and Y. Jiang, *Opt. Fiber Technol.* **83**, 103655 (2024).
14. L. Zhang, J. Zhang, Q. Sheng, C. Shi, W. Shi, and J. Yao, *Opt. Express* **29**, 27048 (2021).
15. S. Fu, X. Zhu, J. Zong, M. Li, A. Chavez-Pirson, and R. A. Norwood, *Opt. Express* **32**, 40991 (2022).
16. A. Schülzgen, L. Li, D. Nguyen, C. Spiegelberg, R. M. Rogo-
jan, A. Laronche, J. Albert, and N. Peyghambarian, *Opt. Lett.* **33**, 614 (2008).
17. J. Zhou, A. Luo, Z. Luo, X. Wang, X. Feng, and B. Guan, *Photonics Res.* **3**, A21 (2015).
18. M. Bernier, V. Michaud-Belleau, S. Levasseur, V. Fortin, J. Genest, and R. Vallée, *Opt. Lett.* **40**, 81 (2015).
19. D. D. Hudson, R. J. Williams, M. J. Withford, and S. D. Jackson, *Opt. Lett.* **38**, 2388 (2013).
20. Y. Lu, X. Jiang, F. Chen, C. Lu, and S. He, *Appl. Sci.* **11**, 2073 (2021).
21. P. Tang, Y. Wang, E. Vicentini, F. Canella, L. M. Molteni, N. Coluccelli, P. Laporta, and G. Galzerano, *J. Lightwave Technol.* **40**, 2489 (2022).
22. J. Ma, Z. Qin, G. Xie, L. Qian, and D. Tang, *Appl. Phys. Rev.* **6**, 021317 (2019).
23. Y. Fang, Y. Ge, C. Wang, and H. Zhang, *Laser Photonics Rev.* **14**, 1900098 (2020).
24. C. Shi, H. Tian, Q. Sheng, W. Shi, Q. Fang, S. Sun, J. Zhang, X. Deng, and J. Yao, *Res. Phys.* **28**, 104594 (2021).
25. M. Leigh, W. Shi, J. Zong, Z. Yao, S. Jiang, and N. Peyghambarian, *Appl. Phys. Lett.* **92**, 181108 (2008).
26. Q. Fang, W. Shi, K. Kieu, E. Petersen, A. Chavez-Pirson, and N. Peyghambarian, *Opt. Express* **20**, 16410 (2012).
27. X. Li, Y. Xu, L. Yang, Y. Cui, Z. Zhou, M. Wang, and Z. Wang, *Opt. Express* **31**, 40991 (2023).
28. H. Luo, J. Li, J. Xie, B. Zhai, C. Wei, and Y. Liu, *Opt. Express* **24**, 29022 (2016).
29. L. Yu, J. Liang, Q. Zeng, J. Wang, X. Luo, J. Wang, P. Yan, F. Dong, X. Liu, Q. Lü, C. Guo, and S. Ruan, *High Power Laser Sci. Eng.* **11**, e53 (2023).
30. X. Wang, P. Zhou, R. Su, H. Xiao, X. Xu, and Z. Liu, *Laser Phys.* **23**, 015101 (2012).
31. W. Lee, J. Geng, S. Jiang, and A. W. Yu, *Opt. Lett.* **43**, 2264 (2018).
32. M. Wang, D. Ouyang, Y. Chen, M. Liu, J. Zhao, X. Liu, and S. Ruan, *Infrared Phys. Technol.* **136**, 105080 (2024).
33. C. Wei, H. Zhang, H. Shi, K. Konynenbelt, H. Luo, and Y. Liu, *IEEE Photonics Technol. Lett.* **29**, 881 (2017).
34. S. Huang, M. Wan, J. Wu, D. Lu, B. Zhang, Y. Zheng, C. Liu, and X. Fang, *Appl. Opt.* **61**, 1791 (2022).
35. S. Huang, T. Zhu, M. Liu, and W. Huang, *Sci. Rep.* **7**, 41988 (2017).
36. G. P. Agrawal and N. A. Olsson, *IEEE J. Quantum Electron.* **25**, 2297 (1989).
37. P. Ma, Y. Miao, W. Liu, D. Meng, and P. Zhou, *Opt. Lett.* **45**, 1974 (2020).